Hindawi
Advances in Civil Engineering
Volume 2020, Article ID 8838989, 14 pages
https://doi.org/10.1155/2020/8838989

Research Article

Effects of Water and scCO$_2$ Injection on the Mechanical Properties of Granite at High Temperatures

Nao Shen,[1,2] **Qiang Zhang**,[3] **Xiaochun Li**,[1] **Bing Bai**,[1] **and Haixiang Hu**[1]

[1]*State Key Laboratory of Geomechanics and Geotechnical Engineering, Institute of Rock and Soil Mechanics, Chinese Academy of Sciences, Wuhan 430071, China*
[2]*University of Chinese Academy of Sciences, Beijing 100049, China*
[3]*Powerchina Huadong Engineering Corporation, Limited, Hangzhou 311122, China*

Correspondence should be addressed to Xiaochun Li; xcli@whrsm.ac.cn

Received 11 August 2020; Revised 9 November 2020; Accepted 1 December 2020; Published 22 December 2020

Academic Editor: Fengqiang Gong

Copyright © 2020 Nao Shen et al. This is an open access article distributed under the Creative Commons Attribution License, which permits unrestricted use, distribution, and reproduction in any medium, provided the original work is properly cited.

Geothermal energy is an important resource to substitute for traditional fossil fuels. The mechanical properties of reservoir rock under the conditions of water and scCO$_2$ injection at different temperatures are crucial for the safety of Enhanced Geothermal Systems. However, the effects of working fluid on the mechanical properties of granite at in situ temperatures are still rarely reported. To reveal the impact mechanisms, conventional triaxial compression experiments were conducted on granite specimens with different confining pressures (2–20 MPa), different pore fluid (10 MPa water or CO$_2$), and different temperatures (25–150°C) in the present study. SEM analyses were applied to the specimens to determine failure surface morphologies after the experiments. The experimental results show that the effective confining pressure, pore fluid, and temperature have significant effects on the strength of granite specimens. The strength of granite increases with the increase of effective confining pressure, with similar granite strength under the same effective confining pressure (dry, water, and CO$_2$). Temperature strengthening of granite is limited by high confining pressure (~15 MPa). Under the effective confining pressure of 5 MPa, temperature weakening occurs on granite specimens when temperature is higher than 90°C. There is fluid diffusion in the specimens during compression. The higher viscosity of water may cause a temporary decrease in effective confining pressure, which may increase the strength of granite. The growth or formation of cracks is mainly observed in quartz and feldspar grains without short-term chemical effects. More visible cracks are observed on the specimens and more volume of fluid is injected under CO$_2$ injection conditions, which may be beneficial to increase the permeability of geothermal reservoir.

1. Introduction

Geothermal energy has been identified as a renewable energy source to substitute for traditional fossil fuels due to its advantages of low carbon emissions, large reserves, and wide distribution [1, 2]. There are four main kinds of geothermal resources: hot dry rock (HDR), geopressured, hydrothermal, and magma resources, among which HDR is an important available geothermal resource. As a notable method of geothermal exploitation, EGS was proposed on the basis of hot dry rock mining technology [3, 4]. However, the high-temperature and high-pressure geological conditions of geothermal reservoirs are a challenge for geothermal development projects. Under these thermo-hydro-mechano-chemical coupling conditions, the mechanical properties of granite are a basic scientific problem that needs to be studied. Laboratory experiments conducted under geothermal conditions can provide basic predictions for actual EGS projects.

Related experimental studies have shown that the mechanical properties of granite are affected by confining pressure, pore pressure, and temperature [5–7]. The effect of the stress state on the mechanical behaviors of granite has been studied widely based on different failure criteria [8–10]. The strength of granite increases with increasing confining pressure [11, 12]. The effect of water injection on the granite

strength has also been studied by many researchers. Wong et al. [13] reviewed the publications that involve the strength and elastic modulus degradation of rocks in the presence of water, pointing out that water content is a significant factor leading to the reduction of strength. The effect of water injection can be the reduction in effective stress and induced crack growth and chemical reaction [14–17]. Compared with water as a working fluid, there is also an idea of using supercritical CO_2 as a working fluid [18]. High temperature can also change the mechanical properties of granite, such as its compressive strength, tensile strength, and elastic modulus, due to thermal expansion and crystal transformations of minerals [7, 19–25]. However, most experiments have been conducted with specimens after thermal treatment, which is not corresponded to the continuous thermal stress conditions of geothermal reservoirs. Furthermore, there is little experimental research on the mechanical properties of granite under in situ fluid injection and high temperature conditions.

The purpose of this article is to reveal the effect of pore fluid (10 MPa water and CO_2) injection on the mechanical behaviors of granite at medium-to-high temperatures (60 to 150°C). Conventional triaxial tests were performed on granite specimens to clarify the mechanical behavior of granite. To determine the microphysical mechanism, the failure surfaces of the posttest specimens were analyzed by scanning electron microscopy (SEM). The long-term chemical effect of pore fluid with rock was studied by geochemical calculations. Finally, the significance of the experimental results for EGS projects is discussed.

2. Experimental Material and Methods

2.1. Specimen Material. The granite specimens used in the present experiments were obtained from Qichun, Hubei Province, China. Petrophysical analysis with X-ray diffraction shows that the granite is composed of 28.42% albite, 21.76% quartz, 45.14% microcline, and 4.68% biotite. On average, the size of the cylindrical specimens is 25 mm in diameter and 50 mm in length with polished ends. The two ends of the granite specimen are perpendicular to the specimen axis, with nonparallelism less than 0.05 mm (Figures 1(a) and 1(b)). A thin section of the intact specimen observed by optical analysis is shown in Figure 1(c). Prior to use, the specimens are well prepared and placed in air at room temperature for several weeks.

2.2. Experimental Setup. Our conventional compression experiments were conducted using a modified in-house shear-flow test apparatus [26], as shown in Figure 2(a). To allow free access of the pore fluid to the ends of the granite specimen, the faces of the two steel plates are grooved both radially and concentrically (Figure 2(b)). The combination of the specimen and plates is packed with a Teflon heat-shrink tube that separates the pore fluid from the confining pressure fluid.

This apparatus consists of an internally heated triaxial testing machine, with silicone oil as the confining medium. The temperature is controlled using a proportional-integral-derivative (PID) progress, ranging from room temperature to 150°C with a resolution of ±0.2°C. The axial load on the specimen is measured directly with an internal submersible load cell. The loading capacity of the axial loading unit is 250 kN, and the displacement rate varies from 0.5 to 50 μm/s. The axial compression of the specimen is measured using two linear variable differential transformers (LVDTs) with a measurement range of 0–5 mm (±2.5 μm). The radial deformation of the specimen is measured using a circumferential strain gauge (10 mm range). The pore fluid pressure and confining pressure are regulated by two servo-controlled volumetric pumps (ISCO pump). A programmable logic controller (PLC) is used to acquire the experimental data and operate the apparatus through a computer.

2.3. Experimental Procedure and Methods. To consider the effects of confining pressure P_c, conventional triaxial compression experiments are conducted on granite specimens under different confining pressure conditions at room temperature ($T \approx 25$°C) and 60°C, with no pore fluid injection ($P_p = 0$). The experiments conducted are listed in Table 1, along with the corresponding experimental conditions.

To study the effect of water/CO_2 and temperature on the mechanical behavior of granite, three series of triaxial compression tests are conducted, that is, dry, water injection, and CO_2 injection. Each series of experiments is performed at 60°C, 90°C, 120°C, and 150°C. The specimens and experimental conditions are compiled in Table 2. For all experiments, the effective stress (P_c–P_p) is fixed at 5 MPa. In consideration of the critical point of CO_2, that is, $T_{crit} = 31.1$°C and $P_{crit} = 7.38$ MPa [27], the injection pressure P_p is fixed at 10 MPa.

Before starting the experiments, the specimen was installed reliably, with pipes connected and displacement sensors (LVDTs and circumferential strain gauge) attached (Figure 2(c)). Then, silicone oil was pumped into the triaxial cell using the air compressor. The temperature was increased to the target value with the outlet valve opened because of thermal expansion of silicone oil. The confining pressure of the triaxial cell was loaded to the target value after the temperature stabilizes. Except for the dry condition, the pore fluid pipes outside the triaxial cell were connected. Then, the pore fluid pipeline was vacuumed by a vacuum pump for half an hour. The injection pressure was loaded to the target value with water or CO_2 pumped to both ends of the specimen, and the specimen was saturated until the volume of the pore fluid pump no longer changed (about one hour). It should be pointed out that, to ensure the dryness of CO_2, we have used high-pressure nitrogen to remove residual water in the pore fluid pipes before the CO_2 injection test. When the temperature was stable again, axial pressure was

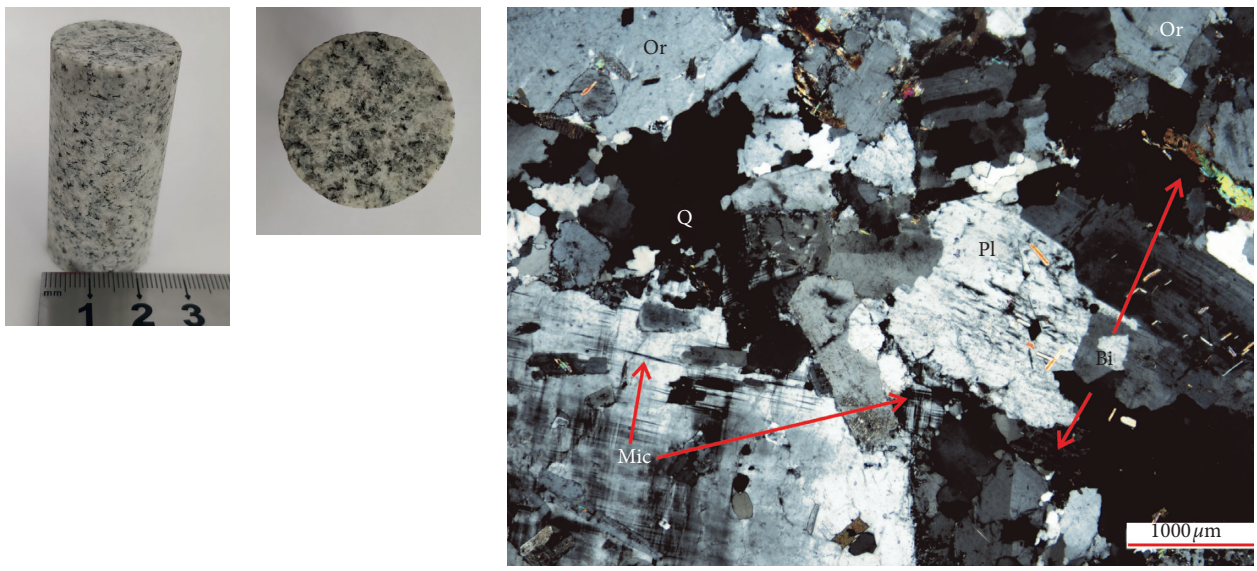

Figure 1: The granite specimens: (a) close-up view of a specimen; (b) end face of a specimen; (c) photomicrograph of a thin section of a pretest specimen (Or: orthoclase, Q: quartz, Mic: microcline, Pl: plagioclase, and Bi: biotite).

loaded on the top of granite specimen at a 5 μm/s displacement rate until the specimen fractured. Finally, the specimen was removed out from the triaxial cell. The distributions of cracks and mineral crystal fractures on the failure surface were observed by SEM.

3. Results

3.1. Mechanical Behavior and Failure Modes of Specimens. To illustrate the effects of confining pressure and temperature on the compressive strength of granite specimens, the experimental results are plotted in Figure 3. This figure shows that the rock strength increases with increasing confining pressure. When a confining pressure of 2 MPa is applied on the specimen, the peak stress ($(\sigma_1-\sigma_3)_{max}$) is 86.0 MPa. The compressive strength increases to 350.9 MPa when 20 MPa confining pressure is applied. Temperature has a significant effect on rock strength under low confining pressure conditions. After the confining pressure reaches 15 MPa, increasing temperature to 60°C has little effect on the strength of granite. It can be seen that both confining pressure and temperature have effects on the strength of granite.

The typical stress-strain curves obtained by conventional triaxial compression experiments under different fluid injection and temperature conditions are presented in Figures 4(a)–4(c). Here, σ_1 and σ_3 are the maximum principal stress and minimum principal stress, respectively. The parameter ε represents axial strain (ε_1) when it takes a positive value and represents radial strain (ε_2) when it takes a negative value. As shown in Figures 4(a)–4(c) , there are four stages, namely, densification, elasticity, yielding, and failure, for the complete stress-strain curves of the granite specimens after experiments. For conditions without fluid injection, increasing temperature enhances the compressive strength of granite below 90°C. The strength of rocks is weakened by increasing temperature to 150°C with a decrease in the axial strain at peak stress (Figure 4(a)). Under the condition that the pore fluid is CO_2, the variation trend of the granite strength with temperature is similar to that under the condition of no fluid injection. Among all experimental results, the granite strength reaches a minimum value of 119.1 MPa under the conditions of 150°C and 10 MPa CO_2 pore fluid (Figure 4(c)). The trends in the rock strength with temperature under different fluid injection conditions are shown in Figure 4(d), with all data fitted by a polynomial ($(\sigma_1-\sigma_3)_{max} = -0.01747T^2 + 3.1466T + 58.9$, $R^2 = 0.66$).

Table 3 lists the mechanical properties of the tested specimens, including peak stress, yield stress, elastic modulus, Poisson's ratio, and axial strain at peak stress. The yield stress is the strength of the specimen when the stress-strain curve deviates significantly from linearity. The elastic modulus is the secant modulus at 50% peak stress. In general, the elastic moduli of the specimens under no fluid injection conditions are larger than those under water and CO_2 injection conditions. Poisson's ratio is the ratio of axial strain to transverse strain at 50% peak stress. Fluid injection decreases Poisson's ratio of rocks, and this decrease is more obvious under the condition of CO_2 injection. The evolution laws of elastic modulus, Poisson's ratio, and axial strain of peak stress with temperature are not obvious.

Postfailure images (Figure 5) of tested specimens are collected after each test with specimens still wrapped by the heat-shrink tube. Brittle shear failure occurs for each tested specimen after the deviatoric stress reaches the peak compressive strength. Under the condition of no fluid injection, significant brittle cracks can be seen on the surfaces of the specimens. There are almost no visible small cracks near the failure surface of specimen #6 (dry, 90°C). Under the condition of fluid injection, more small cracks can be seen near

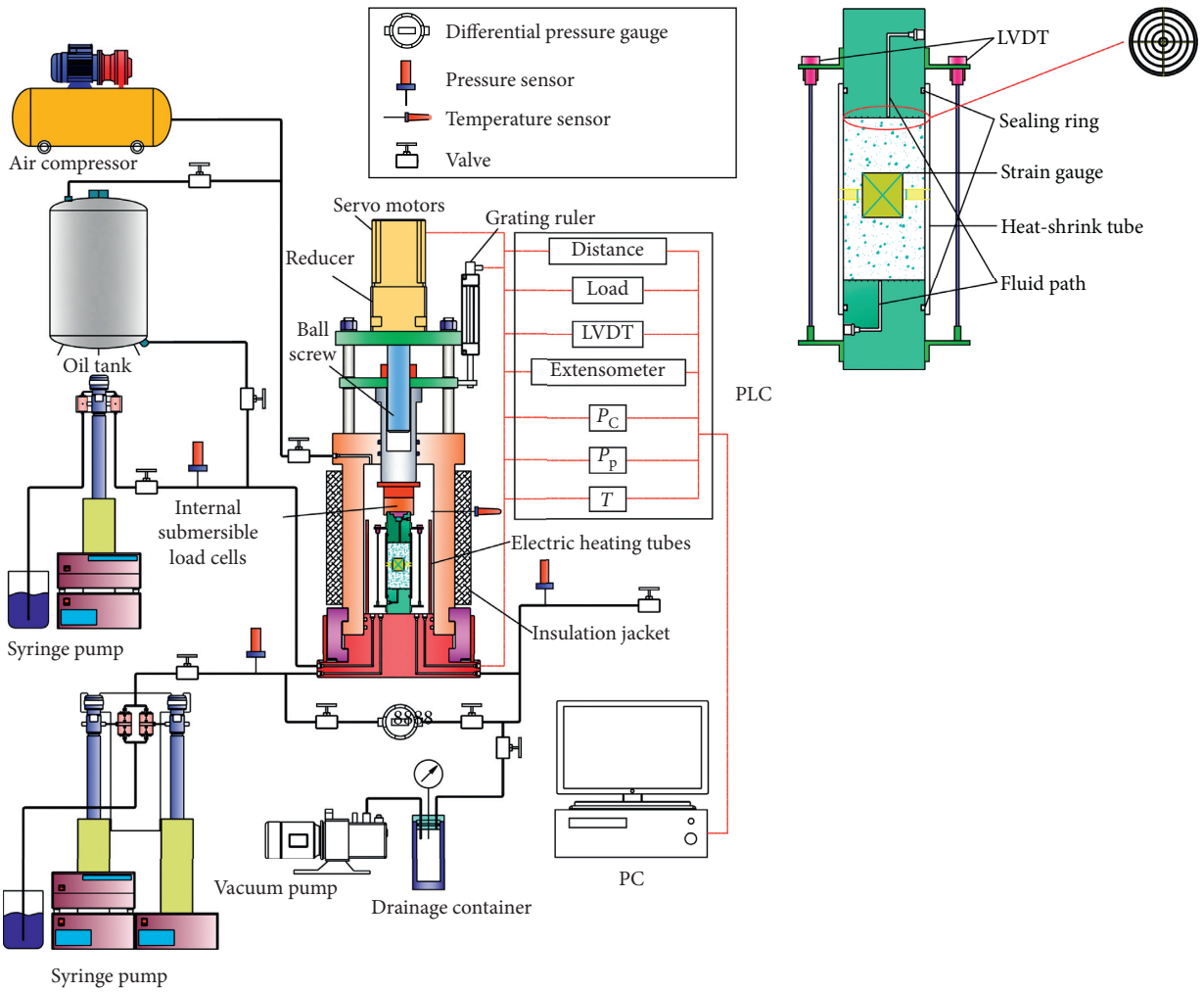

FIGURE 2: The test apparatus: (a) schematic diagram of the apparatus [26]; (b) schematic diagram of the installed granite specimen; (c) close-up view of the installed granite specimen.

Table 1: Conventional triaxial experiments considering the effects of confining pressure and temperature.

Specimen	P_c (MPa)	P_p (MPa)	T (°C)	$(\sigma_1-\sigma_3)_{max}$ (MPa)
T-1	2	0	25	86.0
T-2	2	0	60	170.0
T-3	5	0	25	110.0
#5	5	0	60	176.9
T-4	10	0	25	155.7
T-5	10	0	60	253.4
T-6	15	0	25	311.2
T-7	15	0	60	301.5
T-8	20	0	25	350.9
T-9	20	0	60	355.4

Table 2: Testing conditions for the triaxial compression experiments considering the effect of pore fluid and temperature.

Specimen	P_c (MPa)	P_p (MPa)	Pore fluid	T (°C)
#5	5	0	Dry	60
#6	5	0	Dry	90
#7	5	0	Dry	120
#8	5	0	Dry	150
#9	15	10	Water	60
#10	15	10	Water	90
#11	15	10	Water	120
#12	15	10	Water	150
#13	15	10	CO_2	60
#14	15	10	CO_2	90
#15	15	10	CO_2	120
#16	15	10	CO_2	150

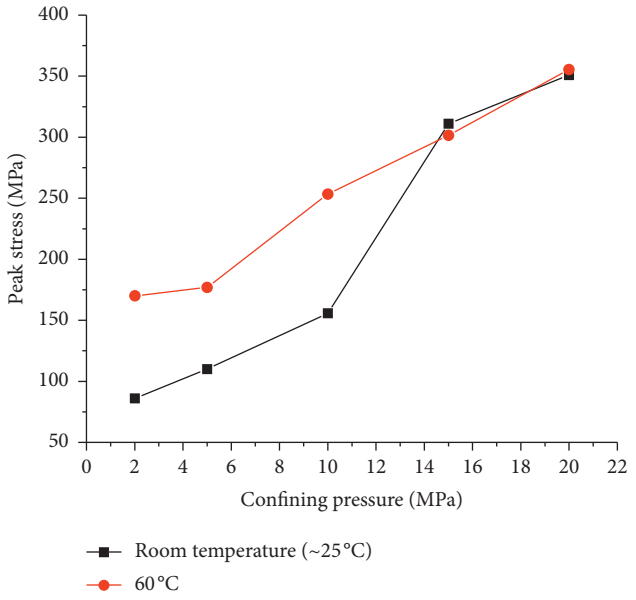

Figure 3: The effects of confining pressure (2, 5, 10, 15, and 20 MPa) and temperature (room temperature and 60°C) on the compression strength of granite specimens.

the failure surfaces (specimens #9–#16 in Figure 5). Especially for specimen #16 (scCO_2, 150°C), a large number of visible small cracks appear near the lower end face of the specimen. Some tested specimens are soaked with silicone oil due to cracking of the heat-shrink tube along failure surface. In consideration of the stable pore pressure during the experiment, it has been indicated that the heat-shrink tube is cracked after the unloading of pore pressure.

3.2. Volumetric Strain and Seepage Behavior of Specimens. The volume of the injected fluid in the sample could be monitored by the ISCO pump. In consideration of the thermal expansion effects of fluid from pump to triaxial cell, the volume data of pore fluid were accurately corrected. It should be noted that these volume data only show the change in pore fluid volume after the axial stress is applied. Under pore fluid injection and different temperature conditions, the volumetric strain (i.e., $\varepsilon_1 + 2\varepsilon_2$) and the injected fluid volume change with the compression of the tested specimens (Figure 6). The whole compression process is divided into four stages. In stage I, the specimens are in the compacted and elastic phases as the volumetric strain increases. As shown in Figures 6(a)–6(d), the fluid volume in the specimens decreases with compaction when the injected fluid is water. When the injected fluid is CO_2, there is an increase of the injected fluid volume in this stage (Figures 6(e)–6(h)). In stage II, the increase in volumetric strain slows down and then begins to decrease corresponding to the yield and destruction phases of the tested specimens (Figure 4). The injected volume of both water and CO_2 increases in this stage. In stage III, the volumetric strain increases suddenly because the axial strain changed too quickly (failure stage). The injected fluid volume is too late to change at this stage. When the axial displacement continued to increase (stage IV), the tested specimens swell suddenly, and the volume of injected fluid reaches the maximum value.

3.3. Microstructural Observations. After each experiment, a small piece (about 25 mm^2) was cut down from the failure surface of each specimen for SEM analysis. The basis of mineral identification in SEM images in this study is from literature [28]. Combined with the XRD analysis results, the main mineral components, that is, quartz, feldspar, and biotite, are observed in the SEM images (Figure 7). Quartz minerals are granular and have a relatively smooth surface. Feldspar minerals are plate-like, while biotite minerals are flake. Brittle failure of quartz and feldspar can be seen from the failure surface, while the biotite undergoes ductile failure caused by shearing. There are many cracks in quartz grains (Figures 7(a)–7(c)), and the numbers and openings of cracks are affected by temperature. Even under different fluid injection conditions, increasing temperature leads to the expansion and connectivity of preexisting cracks in quartz. For feldspar, the fracture morphology seems to be related to the shear direction (Figures 7(d)–7(f)). When the shear direction is at an acute angle with the feldspar cleavage direction, the fracture is stepped (Figure 7(d)). When the two directions are parallel, the destruction of feldspar is most obvious (Figure 7(e)). When the two directions are perpendicular, much mineral debris can be observed on the failure surface (Figure 7(f)). Biotite grains undergo similar damage under

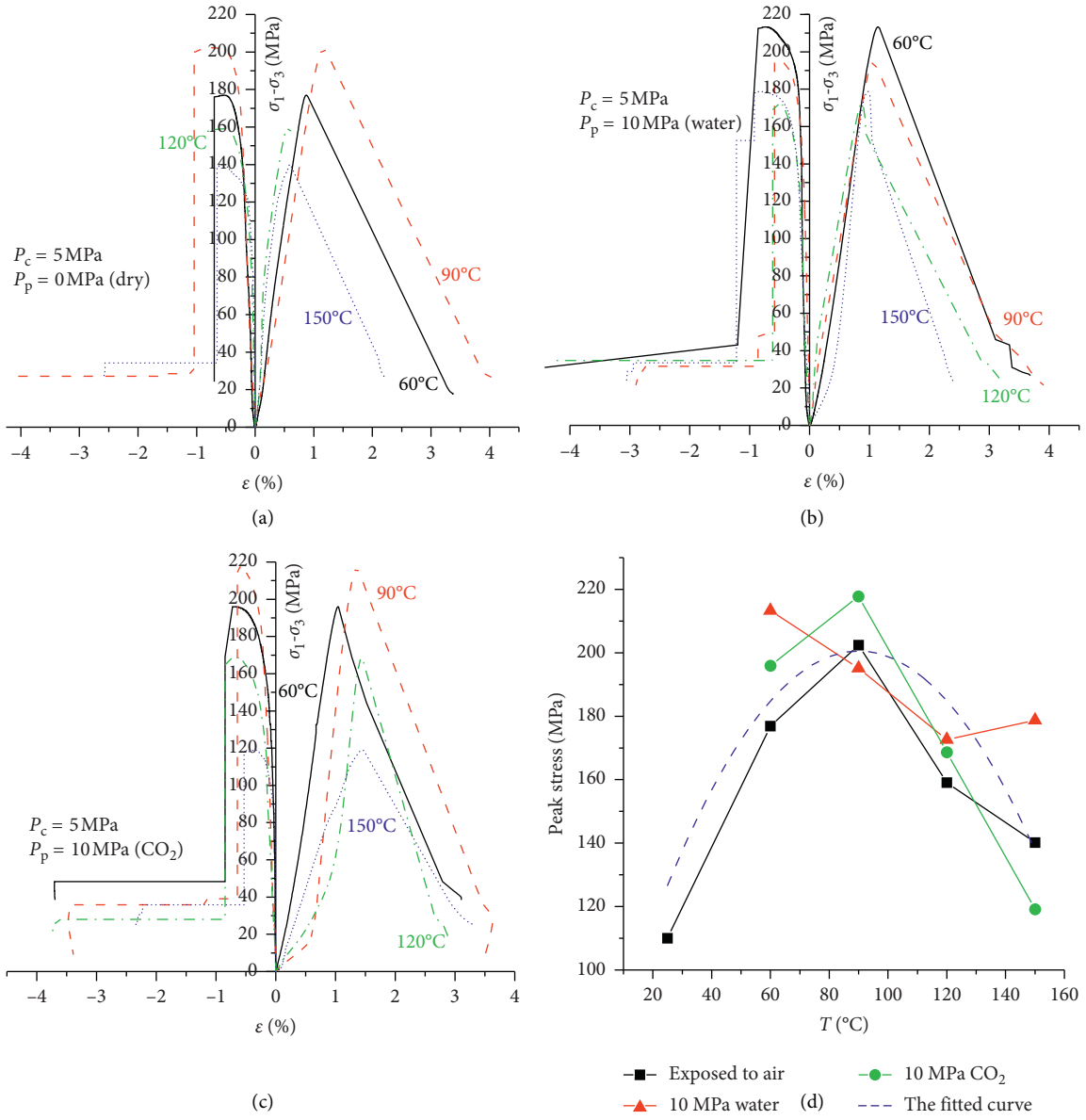

Figure 4: Results of conventional triaxial compression experiments on granite specimens: (a) stress-strain curves of granite specimens under 5 MPa confining pressure and different temperature conditions; (b) stress-strain curves of granite specimens under water injection (10 MPa) and different temperature conditions; (c) stress-strain curves of granite specimens under CO_2 injection (10 MPa) and different temperature conditions; (d) the relationship between the peak stress of granite specimens and the temperature at the same effective confining pressure (5 MPa).

Table 3: Mechanical properties of granite specimens under fluid injection and high temperature conditions.

Specimen	$(\sigma_1-\sigma_3)_{max}$ (MPa)	Yield stress (MPa)	Elastic modulus (GPa)	Poisson's ratio	Axial strain at peak stress
#5	176.9	164.0	22.5	0.353	0.876
#6	202.4	193.8	17.6	0.262	1.173
#7	159.1	133.2	51.3	0.390	0.549
#8	140.2	119.4	40.1	0.179	0.594
#9	213.3	196.7	18.4	0.213	1.142
#10	195.1	187.3	19.5	0.129	1.063
#11	172.6	155.1	24.2	0.288	0.872
#12	178.7	151.4	14.4	0.194	0.975
#13	196.0	183.4	17.8	0.082	1.045
#14	217.8	199.6	12.1	0.133	1.353
#15	168.7	156.5	7.5	0.113	1.438
#16	119.1	112.3	9.2	0.013	1.436

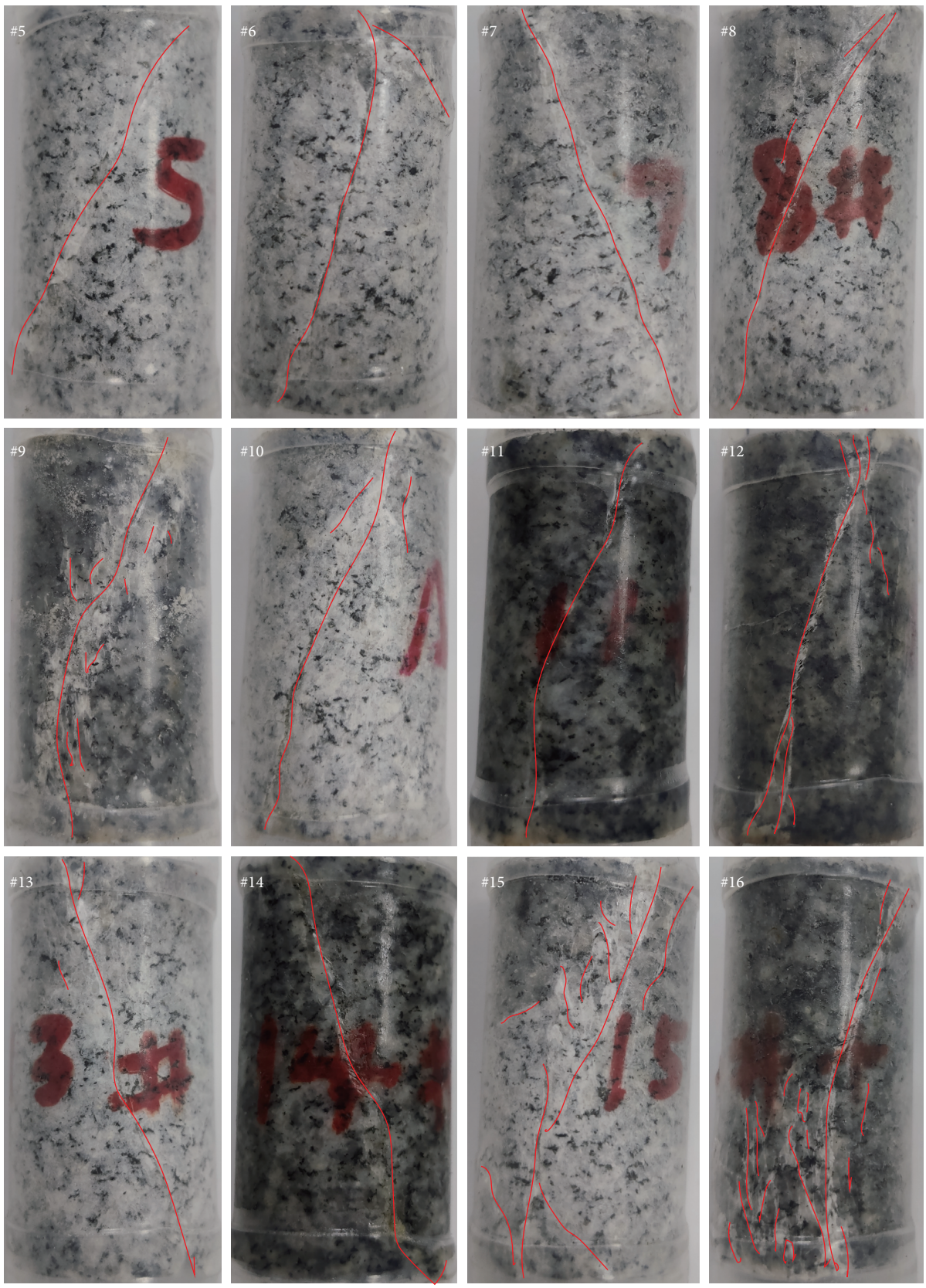

Figure 5: Postfailure images of tested granite specimens. From left to right, the experimental temperature conditions are 60°C, 90°C, 120°C, and 150°C. From top to bottom, the fluid injection conditions are dry, water, and CO_2. The red lines show the fractures on the surface of tested specimens.

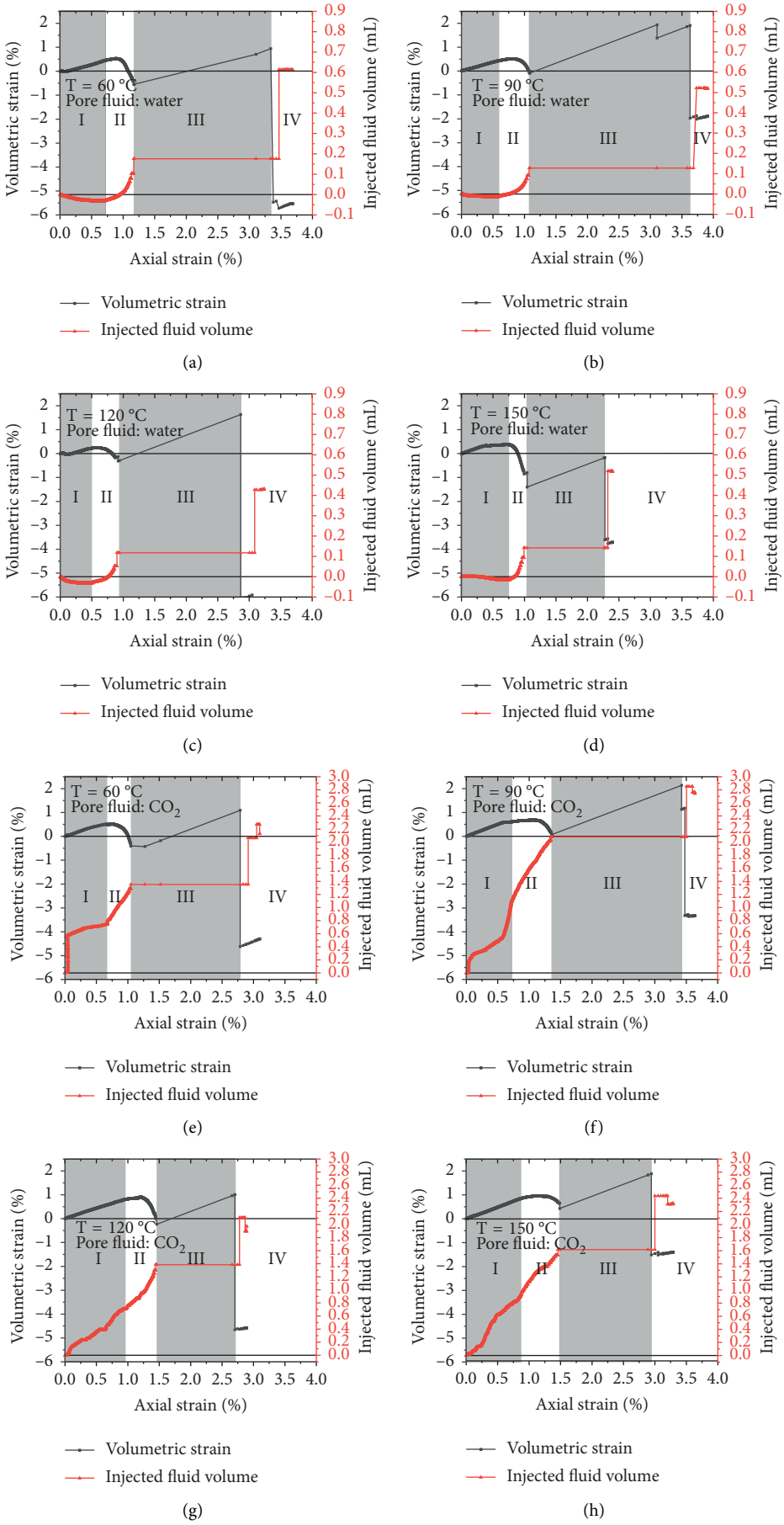

Figure 6: Volumetric strain-axial strain and injected fluid volume curves for the compression experiments under different pore fluid injection and temperature conditions. There are four common stages, that is, stage I, stage II, stage III, and stage IV.

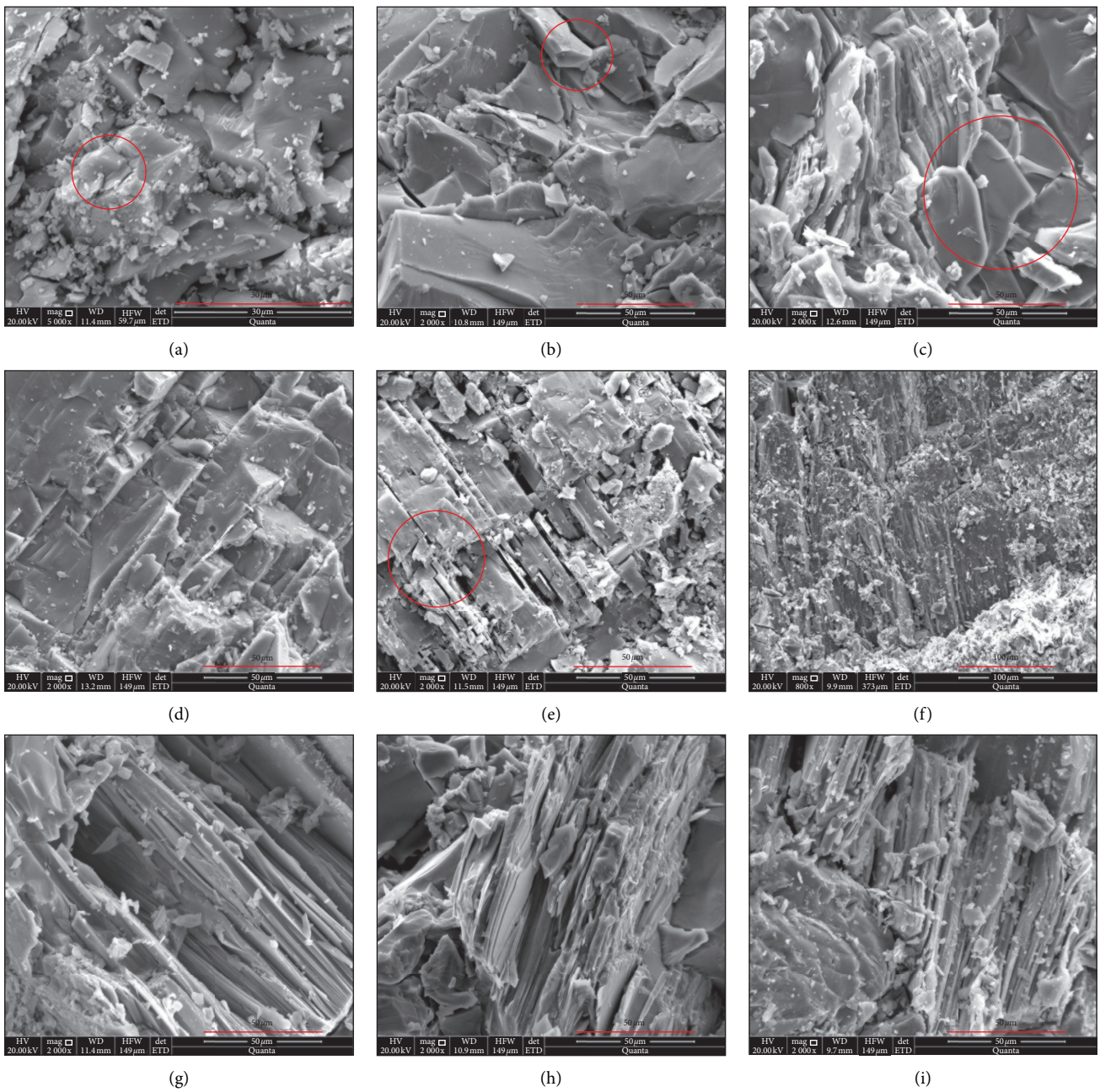

FIGURE 7: SEM images of failure surface of the posttest granite specimens. (a–c) Cracks in quartz under different fluid injection and temperature conditions. (d–e) Shear failure of feldspar under different fluid injection and temperature conditions. (g–i) Shear failure of biotite under different fluid injection and temperature conditions. The cracks are circled in red.

different fluid injection and temperature conditions, with the fracture morphology related to the shear direction (Figures 7(g)–7(i)). No visible evidence shows that mineral corrosion and precipitation occur at the failure surface.

4. Analysis and Discussion

The experimental results in the present study show that the compressive strength of granite obtained by conventional triaxial testing is sensitive to confining pressure (2–20 MPa), temperature (room temperature to 150°C), and pore fluid (dry and 10 MPa water or CO_2). Both the confining pressure and temperature influence the opening and initiation of cracks. The injection of pore fluid reduces the effective confining pressure and may induce the propagation of cracks. The short-term chemical effects are inferred to have little effect on the strength of granite. In the following sections, the influences of effective pressure and temperature on the strength of granite are analyzed. The reasons for different pore fluids (water and CO_2) affecting granite strength were analyzed. Furthermore, the possible long-term effects of reactions between rock and pore fluid are

discussed. Finally, the significance of the experimental results for the EGS projects is discussed.

4.1. Influences of Effective Confining Pressure on Strength. The compressive strengths of many types of rocks have been studied under different confining pressures by means of laboratory tests [7, 12, 15, 29, 30]. It is well known that the strength of rock increases with increasing confining pressure P_c. When pore fluid is injected, the effective confining pressure decreases with increasing pore pressure. In the present study, the effect of confining pressure on the compressive strength of granite is shown in Figure 3. It can be concluded from our experimental data that pore fluid injection reduces the strength of granite under the condition of 15 MPa confining pressure and 60°C (Figures 3 and 4(d)). According to our experimental data, the strengths of dry granite specimens and pore fluid containing granite specimens under the same effective confining pressure (P_c-P_p) and temperature are similar (Figure 4(d)). Although the volume of injected pore fluid changes during compression, the strength of granite is still controlled by the effective confining pressure.

4.2. Effects of Temperature on Triaxial Compressive Strength. The influence of temperature on the mechanical properties of granite has been studied by many researchers [19, 20, 22, 31, 32]. Although the temperature of thermal treatment has been up to 1000°C, most of the experiments were performed to study the mechanical properties of rock after heating. Due to the complexity of granite mineral composition and the different thermal expansion coefficients of various minerals, the mineral expansion occurring at high temperature causes significant thermal stress between minerals, resulting in cracks inside the rock, which seriously affect the mechanical properties of the rock [33–36]. Meier [37] proposed three kinds of competition mechanisms for crack propagation in heated rock: (1) thermal cracking leads to reduced rock strength; (2) a crack tip can be blunted and can inhibit the propagation of the crack; and (3) thermal expansion of minerals closes preexisting cracks and enhances rock strength. Yang et al. [20] concluded that the strength of granite increases due to thermal expansion of mineral grains below 300°C; the boundary cracks and transgranular cracks that occur in feldspar and quartz grains result in decreases in strength at 400–600°C; and the interactions and coalescence of boundary cracks and transgranular cracks result in reductions in strength. The transgranular cracks occurring in quartz grains in thermally treated Westerly granite are due to crystal transformation at 573°C [23].

The mechanical properties of granite under in situ temperature conditions have rarely been studied by previous researchers. Dwivedi et al. [38] studied the mechanical properties of Indian granite at temperatures in the range of 30–160°C. The uniaxial compressive strengths of the tested specimens were 118.2 MPa, 112.8 MPa, 122.4 MPa, 133.3 MPa, and 133.7 MPa at 30°C, 65°C, 100°C, 125°C, and 160°C, respectively. The widths of preexisting cracks observed at in situ temperature by SEM increased below 65°C and then decreased. Kumari et al. [7] conducted a series of triaxial experiments on granite specimens under four different confining pressures (10, 30, 60, and 90 MPa) and four different temperatures (RT, 100, 200, and 300°C). The granite strength under 10 MPa confining pressure increased below 200°C and then decreased, with 196.9 MPa at room temperature and 225.5 MPa at 100°C. Furthermore, the microstructure observed by SEM and optical microscopy showed that no significant thermally induced cracks occurred in preheated specimens up to 200°C.

In this study, the experimental data plotted in Figure 3 show that heating from room temperature to 60°C can enhance the strength of granite under confining pressures not higher than 15 MPa. This effect can be caused by the closure of preexisting cracks due to thermal expansion. Under higher confining pressure, heating to 60°C has little effect on the strength of granite (Figure 3), which may be due to closure of preexisting cracks by the high confining pressure. As shown in Figure 4(d), under dry and CO_2 injection conditions, the compressive strength of the granite specimens increases below 90°C and then decreases. The increase in strength may be due to the closure of preexisting cracks, and the decrease in strength may occur because the continued increase in temperature leads to the growth of cracks and the formation of new cracks. However, this explanation does not apply to the experimental results under water injection conditions, which may be due to the differences in fluid properties.

In this study, granite specimens with a similar porphyrotopic texture are used (Figure 1(b)), with microcline as the phenocrysts and the matrix consisting of quartz, albite, and biotite (Figure 1(c)). According to the SEM images of different minerals in Figure 7, the brittle failure of granite is mainly caused by the brittle failure of quartz and feldspar minerals. The degree of cracking in quartz grains may be affected by temperature. The preexisting cracks and new cracks generated in quartz minerals may contribute to the formation of failure surfaces in granite specimens.

4.3. Effects and Mechanisms of Fluid Penetration: Water versus CO_2. Many studies have shown that water injection and water saturation decrease the strength of the rock due to the reduction in effective stress and the softening effect of pore fluid [5, 15, 30]. The effect of fluid injection on the effective stress is discussed in Section 4.1. Here, we focus on the softening effect of fluid injection on rock. For a more intuitive comparison, the viscosity and density of water and CO_2 under the experimental conditions are listed in Table 4, with data selected from the NIST Chemistry WebBook.

In the present study, the volume of injected fluid changes with volumetric strain, which must be caused by the change

Table 4: The viscosity and density of water and supercritical CO_2 at different temperatures*.

Temperature (°C)	10 MPa water		10 MPa CO_2	
	Viscosity (μPa × s)	Density (kg/m^3)	Viscosity (μPa × s)	Density (kg/m^3)
60	468.65	987.48	23.841	289.95
90	317.06	969.78	21.799	202.93
120	234.62	947.94	22.077	167.31
150	184.86	922.32	22.840	145.56

*Note: all data in this table are selected from the NIST Chemistry WebBook.

Table 5: The volume of injected fluid under different experimental conditions.

	60°C	90°C	120°C	150°C
Water (mL)	0.176	0.128	0.118	0.142
CO_2 (mL)	1.353	2.079	1.384	1.617

in the volume of connected cracks. Although the volume of injected fluid cannot represent the actual crack volume, it does reflect changes in the crack volume. As shown in Figure 6, the volume of injected water decreases in stage I and increases in stage II, which is different from that under the CO_2 injection condition. The increased fluid volume in the specimen at the end of stage II is listed in Table 5. The volume of injected CO_2 is higher than that of water under the same temperature condition. Furthermore, similar to the change in strength with temperature (Figure 4(d)), the higher the peak stress of the specimen is, the larger the volume of injected fluid is. This result means that more pore fluid is needed to weaken the fracture energy when the strength of the specimen is higher [39]. Observing the postfailure images of the tested granite specimens (Figure 5), we find that the aperture of the failure surface increases with increasing peak strength. Due to the high viscosity of water, it may be difficult for water to enter the cracks immediately when the cracks are connected, resulting in a temporary increase in effective confining pressure. This may be the reason for the higher strength of granite at 60°C and 150°C during water injection compared to that under CO_2 injection conditions. According to linear elastic fracture mechanics [40], the lower effective stress induced by the lower viscosity of CO_2 may be the reason for more visible cracks on the specimens under CO_2 injection conditions. In addition, we find that pore fluid injection reduces the elastic modulus of granite and that the weakening effect of CO_2 is more obvious (Table 3).

4.4. Effects of Rock and Fluid Chemical Reactions. The effects of chemical interactions between fluid and granite on the strength of granite should be considered in the long term. Bucher and Stober [41] proved that the dissolution of granite mainly involves plagioclase and biotite and that increasing the temperature to 50°C promotes the dissolution of minerals. Liu et al. [42] proved that the contents of Si, Al, Na, and K in the leachates from granite increase with increasing temperature below 200°C due to the dissolution of quartz and feldspar. Using a Hastelloy C reaction cell at 100°C, Lin et al. [43] demonstrated that the hydrolysis of the plagioclase phase should be mainly responsible for elements dissolved from granite specimens and that rock minerals should be chemically stable in a water-free $scCO_2$ fluid. Under anhydrous conditions, $scCO_2$ fluid is capable of extracting organic matter from rocks [44] but is not a solvent for inorganic materials [18].

Under the experimental conditions of this study, the short-term chemical effects of pore fluids with tested granite specimens are negligible. The long-term dissolution effects of water on granite are analyzed by the geochemical software PHREEQC [45]. According to component analysis of the initial specimens by XRD and optical analysis, we assume that the components of the granite specimens used in this study are albite, quartz, potassium feldspar, and biotite. Under different temperature conditions, the moles of dissolved and precipitated minerals when the dissolution system reaches equilibrium are shown in Figure 8. As illustrated, when the temperature increases, the dissolution amounts of albite and potassium feldspar increase, with a precipitation of quartz and biotite.

4.5. Implications for EGS Projects. Although the temperature of hot dry rock (HDR) geothermal reservoir is generally higher than 200°C, HDR with lower temperature still has value to be developed [46]. According to our experimental data, granite has an obviously lower strength at 150°C when the injected pore fluid is $scCO_2$. The injection of $scCO_2$ produces more cracks in the rock and a greater volume of fluid can be injected, which may increase the heat exchange between fluid and rock. Compared to water as the working fluid, the water-free $scCO_2$ fluid maintains chemical stability in granite. Precipitation is generated when water is injected in the long term, which may block the fluid flow paths. Although injecting CO_2 may also cause precipitation of substances when there is formation water, this is conducive to the storage of CO_2 [42, 43]. Considering that $scCO_2$ is not as efficient a heat carrier as water, we recommend using

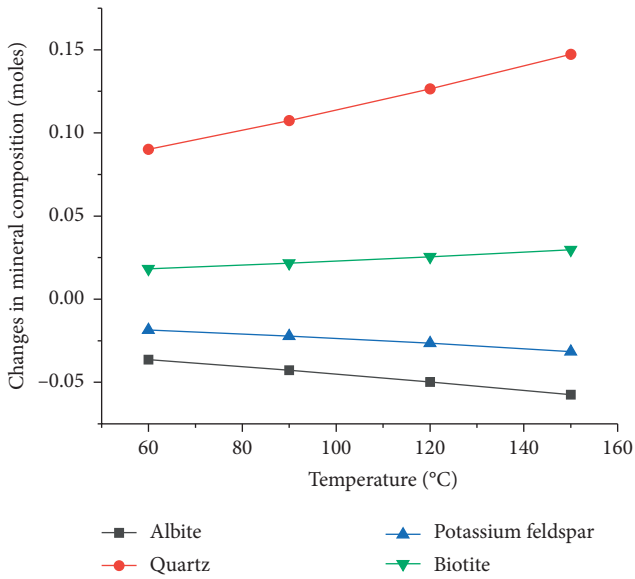

Figure 8: The calculated results for granite compositional changes after water and granite interactions at different temperatures.

$scCO_2$ to increase the permeability of the geothermal reservoir before water injection.

5. Conclusions

A series of conventional triaxial compression experiments were conducted on granite specimens from Qichun, Hubei Province, China, under different confining pressures (2–20 MPa), different injection fluid (10 MPa water or CO_2), and different temperatures (25–150°C). The main conclusions are as follows:

(1) The injection of water and CO_2 reduces the strength and elastic modulus of granite. A greater volume of fluid is injected into the specimen before it breaks when the peak strength is higher, especially for CO_2 injection conditions. More visible cracks are observed on the specimens under CO_2 injection conditions.

(2) There is a critical confining pressure (~15 MPa) for temperature strengthening of granite. Under the effective confining pressure of 5 MPa, the strength of granite changes from temperature strengthening to temperature weakening with the increase of temperature, which may be related to the closure and formation of cracks.

(3) Fluid diffusion in tested specimens occurs during the compression process. Due to the difference in viscosity, it may be difficult for water pressure diffusing along the connected cracks, compared to CO_2 injection. The resulting temporary higher effective confining pressure may increase the strength of granite.

Data Availability

The data used to support the findings of this study are available from the corresponding author upon request.

Conflicts of Interest

The authors declare that they have no conflicts of interest.

Acknowledgments

This study was jointly supported by the National Natural Science Foundation of China (Grant no. 41672252) and the National Key R&D Program of China (Grant no. 2016YFB0600805).

References

[1] H. K. Gupta and S. Roy, *Geothermal Energy: An Alternative Resource for the 21st Century*, Elsevier, Amsterdam, Netherlands, 2006.

[2] M. Martín-Gamboa, D. Iribarren, and J. Dufour, "On the environmental suitability of high- and low-enthalpy geothermal systems," *Geothermics*, vol. 53, pp. 27–37, 2015.

[3] F. Luo, R.-N. Xu, and P.-X. Jiang, "Numerical investigation of fluid flow and heat transfer in a doublet enhanced geothermal system with CO_2 as the working fluid (CO_2 -EGS)," *Energy*, vol. 64, pp. 307–322, 2014.

[4] P. Olasolo, M. C. Juárez, M. P. Morales, S. D´Amico, and I. A. Liarte, "Enhanced geothermal systems (EGS): a review," *Renewable and Sustainable Energy Reviews*, vol. 56, pp. 133–144, 2016.

[5] B. Lee and T. D. Rathnaweera, "Stress threshold identification of progressive fracturing in Bukit Timah granite under uniaxial and triaxial stress conditions," *Geomechanics and Geophysics for Geo-Energy and Geo-Resources*, vol. 2, no. 4, pp. 301–330, 2016.

[6] M. Noorian Bidgoli and L. Jing, "Water pressure effects on strength and deformability of fractured rocks under low confining pressures," *Rock Mechanics and Rock Engineering*, vol. 48, no. 3, pp. 971–985, 2015.

[7] W. G. P. Kumari, P. G. Ranjith, M. S. A. Perera et al., "Mechanical behaviour of Australian strathbogie granite under in-situ stress and temperature conditions: an application to geothermal energy extraction," *Geothermics*, vol. 65, pp. 44–59, 2017.

[8] H. Tian, T. Kempka, N. Xu, and M. Ziegler, *A Modified Mohr-Coulomb Failure Criterion for Intact Granites Exposed to High Temperatures*, pp. 379–393, Springer Berlin Heidelberg, Berlin, Heidelberg, 2013.

[9] L. R. Alejano, J. Arzúa, N. Bozorgzadeh, and J. P. Harrison, "Triaxial strength and deformability of intact and increasingly jointed granite samples," *International Journal of Rock Mechanics and Mining Sciences*, vol. 95, pp. 87–103, 2017.

[10] M. Singh, A. Raj, and B. Singh, "Modified Mohr-Coulomb criterion for non-linear triaxial and polyaxial strength of intact rocks," *International Journal of Rock Mechanics and Mining Sciences*, vol. 48, no. 4, pp. 546–555, 2011.

[11] R. L. Kranz, "The effects of confining pressure and stress difference on static fatigue of granite," *Journal of Geophysical Research*, vol. 85, no. B4, pp. 1854–1866, 1980.

[12] K. Masuda, H. Mizutani, and I. Yamada, "Experimental study of strain-rate dependence and pressure dependence of failure properties of granite," *Journal of Physics of the Earth*, vol. 35, no. 1, pp. 37–66, 1987.

[13] L. N. Y. Wong, V. Maruvanchery, and G. Liu, "Water effects on rock strength and stiffness degradation," *Acta Geotechnica*, vol. 11, no. 4, pp. 713–737, 2016.

[14] S. Zhang, J. Liu, P. Chen, C. Sun, and Y. Wang, "Experimental reseach on mechanical proprties of granite under water-rock coupling," *Chinese Journal of Rock Mechanics Engineering*, vol. 34, no. 3, pp. 520–527, 2015.

[15] C. Cheng, X. Li, S. Li, and B. Zheng, "Failure behavior of granite affected by confinement and water pressure and its influence on the seepage behavior by laboratory experiments," *Materials*, vol. 10, no. 7, p. 798, 2017.

[16] Y. Chen, "Permeability evolution in granite under compressive stress condition," *Geotechnical and Geological Engineering*, vol. 36, no. 8, pp. 641–647, 2018.

[17] S. Miao, M. Cai, Q. Guo, P. Wang, and M. Liang, "Damage effects and mechanisms in granite treated with acidic chemical solutions," *International Journal of Rock Mechanics and Mining Sciences*, vol. 88, pp. 77–86, 2016.

[18] D. W. Brown, "A hot dry rock geothermal energy concept utilizing supercritical CO2 instead of water," in *Proceedings of the Twenty-Fifth Workshop on Geothermal Reservoir Engineering*, pp. 233–238, Stanford University, Stanford, CA, United States, January 2000.

[19] Y. Qin, H. Tian, N.-X. Xu, and Y. Chen, "Physical and mechanical properties of granite after high-temperature treatment," *Rock Mechanics and Rock Engineering*, vol. 53, no. 1, pp. 305–322, 2020.

[20] S.-Q. Yang, P. G. Ranjith, H.-W. Jing, W.-L. Tian, and Y. Ju, "An experimental investigation on thermal damage and failure mechanical behavior of granite after exposure to different high temperature treatments," *Geothermics*, vol. 65, pp. 180–197, 2017.

[21] Q. Sun, W. Zhang, L. Xue, Z. Zhang, and T. Su, "Thermal damage pattern and thresholds of granite," *Environmental Earth Sciences*, vol. 74, no. 3, pp. 2341–2349, 2015.

[22] X.-L. Xu, F. Gao, X.-M. Shen, and H.-P. Xie, "Mechanical characteristics and microcosmic mechanisms of granite under temperature loads," *Journal of China University of Mining and Technology*, vol. 18, no. 3, pp. 413–417, 2008.

[23] M. H. B. Nasseri, B. S. A. Tatone, G. Grasselli, and R. P. Young, "Fracture toughness and fracture roughness interrelationship in thermally treated westerly granite," *Rock Physics and Natural Hazards*, vol. 166, no. 5-7, pp. 801–822, 2009.

[24] L. F. Fan, J. W. Gao, Z. J. Wu, S. Q. Yang, and G. W. Ma, "An investigation of thermal effects on micro-properties of granite by X-ray CT technique," *Applied Thermal Engineering*, vol. 140, pp. 505–519, 2018.

[25] L. F. Fan, Z. J. Wu, Z. Wan, and J. W. Gao, "Experimental investigation of thermal effects on dynamic behavior of granite," *Applied Thermal Engineering*, vol. 125, pp. 94–103, 2017.

[26] Q. Zhang, X. Li, B. Bai, L. Pei, L. Shi, and Y. Wang, "Development of a direct-shear apparatus coupling with high pore pressure and elevated temperatures," *Rock Mechanics and Rock Engineering*, vol. 52, no. 9, pp. 3475–3484, 2019.

[27] G. L. Weibel and C. K. Ober, "An overview of supercritical CO_2 applications in microelectronics processing," *Microelectronic Engineering*, vol. 65, no. 1-2, pp. 145–152, 2003.

[28] J. E. Welton, *SEM Petrology Atlas*, The American Association of Petroleum Geologists, Tulsa, Oklahoma, 2nd edition, 2003.

[29] I. A. H. Ismail and S. A. F. Murrell, "Dilatancy and the strength of rocks containing pore water under undrained conditions," *Geophysical Journal International*, vol. 44, no. 1, pp. 107–134, 1976.

[30] S. J. T. Hangx, C. J. Spiers, and C. J. Peach, "Mechanical behavior of anhydrite caprock and implications for CO_2 sealing capacity," *Journal of Geophysical Research*, vol. 115, no. B7, 2010.

[31] M. H. B. Nasseri, A. Schubnel, and R. P. Young, "Coupled evolutions of fracture toughness and elastic wave velocities at high crack density in thermally treated Westerly granite," *International Journal of Rock Mechanics and Mining Sciences*, vol. 44, no. 4, pp. 601–616, 2007.

[32] S.-Q. Yang, Y.-H. Huang, W.-L. Tian, P.-F. Yin, and H.-W. Jing, "Effect of high temperature on deformation failure behavior of granite specimen containing a single fissure under uniaxial compression," *Rock Mechanics and Rock Engineering*, vol. 52, no. 5, pp. 2087–2107, 2019.

[33] Z. Zhao, "Thermal influence on mechanical properties of granite: a microcracking perspective," *Rock Mechanics and Rock Engineering*, vol. 49, no. 3, pp. 747–762, 2016.

[34] M. Takarli, W. Prince, and R. Siddique, "Damage in granite under heating/cooling cycles and water freeze-thaw condition," *International Journal of Rock Mechanics and Mining Sciences*, vol. 45, no. 7, pp. 1164–1175, 2008.

[35] L. F. Fan, J. W. Gao, and X. L. Du, "Thermal cycling effects on micro-property variation of granite by a spatial micro-observation," *Rock Mechanics and Rock Engineering*, vol. 53, pp. 2921–2928, 2020.

[36] L. Fan, J. Gao, X. Du, and Z. Wu, "Spatial gradient distributions of thermal shock-induced damage to granite," *Journal of Rock Mechanics and Geotechnical Engineering*, vol. 12, no. 5, pp. 917–926, 2020.

[37] T. Meier, "The influence of temperature on Mode II fracture toughness using the punch-through shear with confining pressure experiment," in *71st EAGE Conference and Exhibition incorporating SPE EUROPEC*, vol. 2009, Amsterdam , Netherlands, June 2009.

[38] R. D. Dwivedi, R. K. Goel, V. V. R. Prasad, and A. Sinha, "Thermo-mechanical properties of Indian and other granites," *International Journal of Rock Mechanics and Mining Sciences*, vol. 45, no. 3, pp. 303–315, 2008.

[39] B. Deng, G. Yin, M. Li et al., "Feature of fractures induced by hydrofracturing treatment using water and L-CO_2 as fracturing fluids in laboratory experiments," *Fuel*, vol. 226, pp. 35–46, 2018.

[40] H. Deng, J. Li, J. Liu, M. Zhu, J. Guo, and T. Lu, "Research on propagation of compression shear fracture in rocks considering fissure water pressure," *Rock Soil Mechanics*, vol. 32, no. S1, pp. 297–302, 2011.

[41] K. Bucher and I. Stober, "Water-rock reaction experiments with black forest gneiss and granite," in *Water-Rock Interaction*, I. Stober and K. Bucher, Eds., pp. 61–95, Springer Netherlands, Dordrecht, Netherlands, 2002.

[42] L. Liu, Y. Suto, G. Bignall, N. Yamasaki, and T. Hashida, "CO_2 injection to granite and sandstone in experimental rock/hot water systems," *Energy Conversion and Management*, vol. 44, no. 9, pp. 1399–1410, 2003.

[43] H. Lin, T. Fujii, R. Takisawa, T. Takahashi, and T. Hashida, "Experimental evaluation of interactions in supercritical CO_2/water/rock minerals system under geologic CO_2 sequestration conditions," *Journal of Materials Science*, vol. 43, no. 7, pp. 2307–2315, 2008.

[44] I. Okamoto, X. Li, and T. Ohsumi, "Effect of supercritical CO_2 as the organic solvent on cap rock sealing performance for underground storage," *Energy*, vol. 30, no. 11-12, pp. 2344–2351, 2005.

[45] D. L. Parkhurst and C. A. J. Appelo, "Description of input and examples for phreeqc version 3: a computer program for speciation, batch-reaction, one-dimensional transport, and

inverse geochemical calculations," *Techniques and Methods*, p. 519, Reston, Reston, VA, 2013.

[46] Y. Zhao, Z. Feng, B. Xi, J. Zhao, Z. Wan, and A. Zhou, "Prospect of HDR geothermal energy exploitation in Yangbajing, Tibet, China, and experimental investigation of granite under high temperature and high pressure," *Journal of Rock Mechanics and Geotechnical Engineering*, vol. 3, no. 3, pp. 260–269, 2011.